

Using the mid-Holocene 'greening' of the Sahara to narrow acceptable ranges on climate model parameters

Hopcroft, Peter; Valdes, Paul J.; Ingram, William

DOI:
[10.1029/2020GL092043](https://doi.org/10.1029/2020GL092043)

License:
Creative Commons: Attribution (CC BY)

Document Version
Publisher's PDF, also known as Version of record

Citation for published version (Harvard):
Hopcroft, P, Valdes, PJ & Ingram, W 2021, 'Using the mid-Holocene 'greening' of the Sahara to narrow acceptable ranges on climate model parameters', *Geophysical Research Letters*, vol. 48, no. 6, e2020GL092043. <https://doi.org/10.1029/2020GL092043>

[Link to publication on Research at Birmingham portal](#)

General rights

Unless a licence is specified above, all rights (including copyright and moral rights) in this document are retained by the authors and/or the copyright holders. The express permission of the copyright holder must be obtained for any use of this material other than for purposes permitted by law.

- Users may freely distribute the URL that is used to identify this publication.
- Users may download and/or print one copy of the publication from the University of Birmingham research portal for the purpose of private study or non-commercial research.
- User may use extracts from the document in line with the concept of 'fair dealing' under the Copyright, Designs and Patents Act 1988 (?)
- Users may not further distribute the material nor use it for the purposes of commercial gain.

Where a licence is displayed above, please note the terms and conditions of the licence govern your use of this document.

When citing, please reference the published version.

Take down policy

While the University of Birmingham exercises care and attention in making items available there are rare occasions when an item has been uploaded in error or has been deemed to be commercially or otherwise sensitive.

If you believe that this is the case for this document, please contact UBIRA@lists.bham.ac.uk providing details and we will remove access to the work immediately and investigate.

Geophysical Research Letters



RESEARCH LETTER

10.1029/2020GL092043

Key Points:

- A wide range of proxy data agree in showing a mid-Holocene “green Sahara”
- General circulation models (GCMs) struggle to simulate this
- Bayesian tuning of a GCM succeeds for the mid-Holocene, finding the improvement has little impact on the present-day simulation.

Supporting Information:

- Supporting Information S1

Correspondence to:

P. O. Hopcroft,
p.hopcroft@bham.ac.uk

Citation:

Hopcroft, P. O., Valdes, P. J., & Ingram, W. (2021). Using the mid-Holocene “greening” of the Sahara to narrow acceptable ranges on climate model parameters. *Geophysical Research Letters*, 48, e2020GL092043. <https://doi.org/10.1029/2020GL092043>

Received 9 DEC 2020

Accepted 6 FEB 2021

Using the Mid-Holocene “Greening” of the Sahara to Narrow Acceptable Ranges on Climate Model Parameters

Peter O. Hopcroft¹ , Paul J. Valdes² , and William Ingram³ 

¹School of Geography, Earth & Environmental Sciences, University of Birmingham, Birmingham, UK, ²Bristol Research Initiative for the Dynamic Global Environment, School of Geographical Sciences, University of Bristol, University Road, Bristol, UK, ³Met Office Hadley Centre, Exeter, UK

Abstract During the early to mid-Holocene vegetation expanded to cover much of the present-day Sahara. Although driven by a well-understood difference in the orbital configuration, general circulation models have generally failed to simulate the required rainfall increase. One possible explanation is the presence of systematic biases in the representations of atmospheric convection which might also impact future projections. We employ a Bayesian method to learn from an ensemble of present day and mid-Holocene simulations that vary parameters in the convection, boundary layer and cloud schemes. The model can reproduce the “Green Sahara” rainfall if mixing between convective plumes and the environment is increased in the upper troposphere relative to lower down. This does not appreciably impact the present day simulation, meaning that the paleoclimate reconstructions are able to narrow constraints on suitable parameter ranges. This suggests that other uncertain components of climate models could be targeted in this way.

Plain Language Summary General circulation models are complex computational representations of the Earth's climate system. Run on supercomputers, these can be used to predict future climate change. Past climate changes can also be used to test climate models. One example of this is the “greening” of the Sahara around 11,000–4,000 years ago. Almost all models fail to capture the amplitude of the so-called “Green” Sahara. One possible reason for this is that small scale features such as clouds and storms in the atmosphere must be approximated using parametrizations. These parametrizations are poorly constrained by available climate observations and they thus potentially introduce errors in predictions of past or future climate changes. In this work we show that the “greening” can be simulated accurately when the parametrizations are tuned not only with present day observed climate fields, but additionally with the past “green” Sahara state. This suggests that climate model parametrizations may be significantly improved and uncertainties reduced if climate states from the past are used in developing climate models.

1. Introduction

The hydrological cycle response in a warming climate will be a major driver of future socio-economic impacts (Hoegh-Guldberg et al., 2018). Projections from general circulation models (GCMs: the most detailed and physically based models of the global climate system) consistently predict a warmer future almost everywhere, but precipitation projections are much more divergent, especially in the tropics (Allen & Ingram, 2002; Chadwick et al., 2016; Kent et al., 2015; Rowell et al., 2016).

Much of the uncertainty in future precipitation change is related to processes associated with clouds and convection. In reality these physical processes occur over spatial scales up to 10s of km. In contrast, most GCMs have a resolution of around 150–200 km. Processes such as convection must therefore be parametrized, but all parametrizations are approximations, and the structure of many parametrizations is unavoidably far simpler than reality, leaving no way to choose a parameter value a priori or directly from observations (e.g., Stensrud, 2007).

Paleoclimate changes can provide valuable “out-of-sample” tests for modeling the climate system (Harrison et al., 2015; Schmidt et al., 2014; Tierney et al., 2020; Valdes, 2011; Zhu et al., 2020). This is because past climate states provide examples of both fast and gradual changes that are larger in amplitude than historical climate changes and are therefore more comparable in amplitude to expected future climate change.

© 2021. The Authors.

This is an open access article under the terms of the [Creative Commons Attribution](https://creativecommons.org/licenses/by/4.0/) License, which permits use, distribution and reproduction in any medium, provided the original work is properly cited.

To be useful in this way, a paleoclimate state or transition must be associated with a good understanding of both the underlying forcings (e.g., a change in greenhouse gas levels or a change in orbit) and the resultant impacts in the climate system.

The early to mid-Holocene (around 11,000–4,000 years before present) is frequently highlighted as such a period (Biasutti et al., 2018; Braconnot et al., 2012; Harrison et al., 2015). This is because the ultimate forcing during this time was a very well-understood change in the configuration of Earth's orbit (Berger & Loutre, 1991). The resulting increase in northern hemisphere summer insolation drove enhanced monsoon circulation and precipitation (Kutzbach & Street-Perrott, 1985). This led to a so-called “Greening” of the Sahara (e.g., Claussen et al., 2017). This is evidenced by the development of savanna or steppe-like vegetation (Hély et al., 2014), expansion of lakes and rivers (Kohfeld & Harrison, 2000; Skonieczny et al., 2015), a reduction in dust deposited over the Atlantic (de Menocal et al., 2000; Williams et al., 2016) and the presence of neolithic settlements and domesticated animals (Manning & Timpson, 2014).

Pollen and macro-fossil evidence suggests that annual mean precipitation increased by $1.1 \text{ mm day}^{-1} \pm 0.1$ (Bartlein et al., 2011) relative to the present day (mean \pm standard error for 15–30°N). There is some uncertainty on the spatial pattern of change, with earlier compilations of pollen suggesting a relatively uniform vegetation change (Hoelzmann et al., 1998), while more recent datasets suggest greater changes in vegetation in the South compared with further North (Hély et al., 2014). The pollen samples have been integrated with a vegetation model to infer climate, showing the same overall precipitation increase (Wu et al., 2007). A larger rainfall increase of around 1.5 (0.9–2.8) mm day^{-1} has been inferred from marine core leaf-wax hydrogen isotope ratios (Tierney et al., 2017). A recent isotope-enabled modeling study suggests these isotope changes are consistent with a slightly smaller precipitation increase (Thompson et al., 2021). Despite these uncertainties, all lines of evidence agree on a minimum increase in precipitation of at least 0.7 mm day^{-1} (Joussaume et al., 1999) that enabled vegetation to grow across much of the present-day Sahara (Jolly et al., 1998; Pachur & Holzmann, 1991; Peyron et al., 2006; Ritchie & Haynes, 1987; Street-Perrott et al., 1990).

All GCM simulations driven with the orbital configuration for 6,000 years before present (6 ka BP), simulate an increase in precipitation, but almost always much smaller than these pollen observations imply over the Sahara itself (Braconnot et al., 2007, 2012; Brierley et al., 2020; Joussaume et al., 1999). This is also true when dynamic vegetation and/or dynamic dust processes are enabled (Harrison et al., 2015; Hopcroft & Valdes, 2019; Perez-Sanz et al., 2014). In contrast, when significant changes in the land surface albedo and/or significant reductions in dust aerosols are specified, sufficient rainfall can be simulated (e.g., Levis et al., 2004; Pausata et al., 2016; Skinner & Poulsen, 2016).

Saharan dust particles are less absorbing than is prescribed in most climate models which tend to use outdated radiative properties (Albani & Mahowald, 2019; Hopcroft & Valdes, 2019). A significant dust reduction during the mid-Holocene probably did not appreciably enhance convective precipitation (Hopcroft & Valdes, 2019). Moreover, the reduction in dust loading would have altered cloud formation through dust-cloud interactions, and this has been shown to reduce stratiform precipitation (Thompson et al., 2019). Land-surface feedbacks can efficiently drive the monsoon northwards (Levis et al., 2004; Skinner & Poulsen, 2016; Texier et al., 2000) but there is little agreement on how the “greening” of the Sahara should be configured in models (Chen et al., 2020; Hopcroft et al., 2017; Lu et al., 2018; Street-Perrott et al., 1990; Texier et al., 2000). It is thus not trivial to judge whether or not a sufficient precipitation enhancement is achieved for the right reasons in model simulations of the mid-Holocene. The model-data disparity over North Africa has persisted for several decades across multiple GCMs (Biasutti et al., 2018). This suggests systematic biases that either require more detailed physical representations or a different approach to parameter choices.

In this work, we use the atmospheric component of the coupled GCM HadCM3 (Gordon et al., 2000; Pope et al., 2000; Valdes et al., 2017) which also does not simulate a “greening” of the Sahara under mid-Holocene boundary conditions (Braconnot et al., 2007). We use this GCM to evaluate what the model failure may reveal about the representation of precipitation in GCMs and to compare the parametric constraints from present-day and mid-Holocene climatic conditions.

2. Methods

2.1. General Circulation Model and Boundary Conditions

We use the Met Office Hadley Center atmosphere model 3 (HadAM3) with the MOSES 2.1 land surface scheme and prescribed vegetation cover (Essery et al., 2003; Pope et al., 2000), specifically HadAM3B-M2.1aN (Valdes et al., 2017). This GCM has horizontal resolution of $3.75 \times 2.5^\circ$ (longitude-latitude) with 19 vertical levels. HadAM3 uses the mass-flux convection scheme by Gregory and Rowntree (1990) which is comparable in complexity to schemes used in several other GCMs (Maraun & Widmann, 2018; Stensrud, 2007). Relative to the published configuration of the model (here labeled ORIG), a revised (REV) model version was developed here that includes a humidity-dependence of the mixing and forced detrainment from convection following Derbyshire, et al. (2011), as implemented in more recent Hadley Centre models.

The preindustrial setup follows that of Valdes et al. (2017) with prescribed observed present-day vegetation coverage (Loveland et al., 2000) and preindustrial levels of greenhouse gases (CO_2 , CH_4 and N_2O). We use 1981–2010 climatological sea-surface temperatures (SSTs) and sea-ice from HadISST (Rayner et al., 2003, updated to 2010). For the mid-Holocene, the orbital parameters are modified for the conditions of 6 ka before present (BP) (Berger & Loutre, 1991). Sea surface temperatures (SST) and sea-ice are modified by adding the 6 ka minus preindustrial difference as simulated with the coupled model HadCM3B-M2.1aD, to the preindustrial HadISST climatology. The simulations setup is summarized in Table S1.

Today, the Sahara has a surface albedo of around 0.35 (Loeb et al., 2012). A reduction in albedo would strengthen the monsoon (Boos & Storelmo, 2016; Charney, 1975; Street-Perrott et al., 1990; Texier et al., 2000). The mid-Holocene “greening” involved the northwards expansion of grasses and shrubs (Jolly et al., 1998; Hély et al., 2014). Satellite observations show that these biomes have an albedo of 0.17–0.25 when precipitation is in the range reconstructed for the “greening” (i.e., 1.1 mm day^{-1} Bartlein et al., 2011), see supporting information S1 and Figure S1. The Sahel which is at the periphery of the present-day West African monsoon is in the upper part of this range (0.2–0.3). This may present the best analogue for the mid-Holocene “greening.” This higher end is also consistent with mid-Holocene simulations with dynamic vegetation and soils (e.g., Claussen & Gayler, 1997; Vamborg et al., 2011). Many model studies have prescribed a value at the very lower end of 0.15 (Chandan & Peltier, 2020; Levis et al., 2004; Pausata et al., 2016; Skinner & Poulsen, 2016), which is typically seen in regions of higher rainfall of $2.0\text{--}3.0 \text{ mm day}^{-1}$.

We do not use the HadCM3B-M2.1aD dynamic vegetation scheme as it is overly sensitive to arid conditions (Hopcroft et al., 2017). Instead bare soil in the Sahara region (from $10\text{--}35^\circ\text{N}$, $30^\circ\text{W}\text{--}50^\circ\text{E}$) is replaced with grasses and shrubs with a total fractional coverage of 50%. This produces a surface albedo of 0.27 relative to 0.31 in the preindustrial simulation. This a relatively conservative change for the period since it is at the upper end of the range discussed above.

2.2. Perturbed Parameter Ensemble

We introduce a new variable E into HadAM3 which controls the vertical dependence of entrainment and mixing detrainment—the mixing of environmental air into the convecting air, and of convecting air into its environment. By default, the entrainment rate decays with altitude in proportion to pressure. This was intended as an ad-hoc representation of larger clouds, which proportionally mix less with their surrounding, reaching higher (Gregory & Rowntree, 1990). With the new parameter E we relax this assumption. Increasing E increases the upper troposphere entrainment values and reduces those near to the land surface. A value of zero returns the default proportional dependence on pressure (see supporting information S2).

We configured a 150-member perturbed parameter ensemble using the REV configuration of HadAM3. Eleven GCM parameters within the convection, boundary layer or large-scale cloud schemes were sampled. This includes three new parameters: E which controls the vertical profile of entrainment and detrainment, r_{det} which sets the sensitivity of forced detrainment to the buoyancy gradient (Derbyshire et al., 2011), and α_{det} which sets the sensitivity of detrainment to relative humidity (Derbyshire et al., 2011). The 11 model parameters are assigned different values globally leading to 150 paired ensemble members of preindustrial and mid-Holocene simulations. The parameter definitions and ranges used are given in Table S2 and

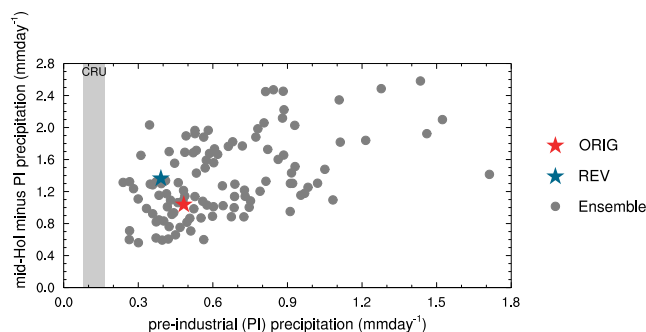


Figure 1. ORIG (red), REV (blue) and ensemble (gray) simulated JJAS precipitation in North Africa (20°W–30°E, 15°N–30°N) against the simulated mid-Holocene minus preindustrial precipitation (mm day^{-1}) change. The observed precipitation in this region from CRU (Harris et al., 2014) based on years 1961–1990, is indicated by the shaded gray bar. The impact of using present-day versus preindustrial precipitation observations is likely to be small and less important than differences due to model biases and due to significant spatial gaps in the early instrumental observations.

illustrated schematically in Figure S2. The evaluations are selected using a Latin hypercube method (McKay et al., 1979), which distributes the parameter samples optimally across the 11-dimensional state space.

2.3. Statistical Modeling and Parameter Tuning

We used a Gaussian process emulator (e.g., Kennedy & O'Hagan, 2001) to construct a statistical representation of the perturbed parameter ensemble of GCM simulations. Emulators have been extensively used in analyzing complex numerical models like GCMs (Edwards et al., 2019; McNeall et al., 2016; Rougier et al., 2009; Sexton et al., 2012). The emulator represents some output as a linear function of the input parameter values combined with a Gaussian process (Roustant et al., 2012). In this way, the emulator interpolates in multidimensional parameter space to predict the GCM response at any combination of input parameter values. Further details are given in supporting information Text S3.

We use a Bayesian method (see supporting information Text S3.2) to update the model parameters based on the mid-Holocene paleoclimate reconstructions. In a Bayesian method we compute a posterior probability distribution function (PDF) on the model parameters based on the prior

PDF and the likelihood (e.g., Rougier, 2007). The prior is taken as the current model version and the likelihood quantifies the performance of the GCM for selected climate outputs such as simulated precipitation. Thus we condition the model parameters with the present-day observed climate variables and optionally the mid-Holocene rainfall increase.

The posterior PDF must be approximated using a Markov chain Monte Carlo method (Gilks et al., 1995) and since the MCMC algorithm requires many thousands of iterations, we use the emulator in place of the full GCM. We perform this process twice. First including four observational targets for the present day (Table S3) and second adding to this the mid-Holocene absolute precipitation over North Africa inferred from pollen data (Bartlein et al., 2011). Thus we derive a new parameter set suitable for both present and mid-Holocene conditions, which is different to Su and Neelin (2005) who used different parameter sets for the two time periods.

3. Results

3.1. Sampling Convection, Clouds and Boundary Layer within a Global Model

The resultant precipitation anomalies for the 112 simulations that completed 50 model years are averaged over North Africa (20°W–30°E by 15–30°N) in Figure 1. This region of North Africa includes many of the fossil pollen sites. All model simulations overestimate present-day precipitation in Africa and in North Africa in particular. This is a systematic bias in HadAM3 (Valdes et al., 2017). Part of which is due to an underestimation of the soil albedo in the Sahara region in the model. The simulated difference for mid-Holocene minus preindustrial in precipitation in this region ranges from 0.7 mm day^{-1} to 2.6 mm day^{-1} for JJAS, when most precipitation falls. Many ensemble members with the preindustrial precipitation similar to the original (around 0.5 mm day^{-1}), have much higher increases of about 2.0 mm day^{-1} for the mid-Holocene. The weak correlation between the two axes in Figure 1 shows that different factors influence precipitation in the preindustrial compared with the precipitation difference between the two time periods.

The parameter dependence of the mid-Holocene precipitation anomaly is shown in Figure S3. The most obvious relationship is with E , for which higher values result in larger changes. E controls the vertical profile of entrainment and detrainment, which is the rate of mixing of convective clouds with the surrounding air masses. In many models entrainment decays with altitude. High values of E increase the upper level entrainment and reduces it near the land surface. This produces a wetter mid-Holocene in North Africa.

The Gaussian process emulator is used to calculate influence of varying each parameter value individually on the simulated precipitation change over North Africa for the mid-Holocene. The result of this is shown

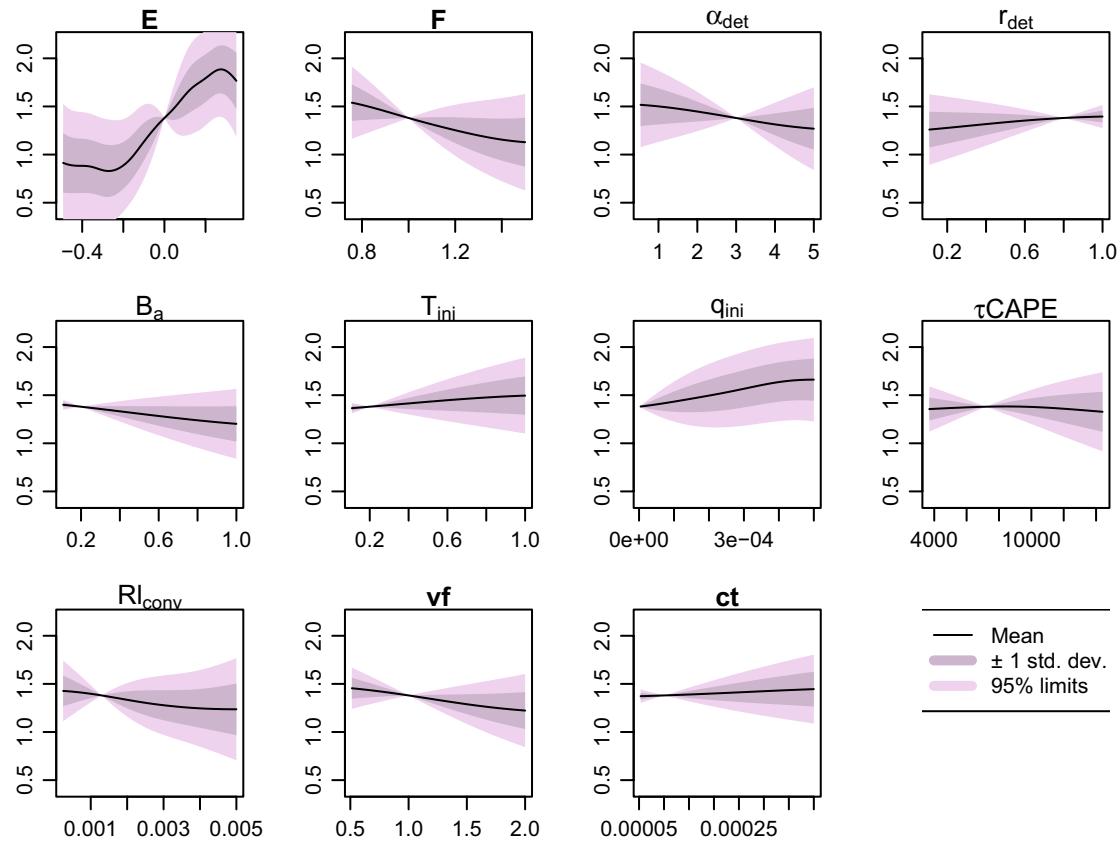


Figure 2. Emulator prediction of JJAS mean precipitation change (mid-Holocene minus preindustrial) over 15°N–30°N by 20°W–30°E. Dependence of the JJAS precipitation difference on each individual model parameter. In each panel that parameter is varied across the range, whilst the remaining 10 parameters are held at their default values. The uncertainty ranges (± 1 standard deviation and the 95% intervals) are as reported by the emulator and collapse to zero at the point in parameter space at which the climate model has been run before. These single parameter sampling evaluations are from the emulator based on all members of the ensemble simulations performed with the GCM. The error bars are a function of distance from points in state-space that have already been evaluated with the GCM. GCM, general circulation model.

in Figure 2 and the emulator skill is evaluated in Figure S4. We find that E is the dominant parameter. We examined the parameter dependence of the West African monsoon in the preindustrial ensemble members (over 5–15°N) (Figure S5). This shows that the parameters which exert the strongest control on precipitation in this monsoon region (q_{ini} , ct and α_{det}) are not the same as for the mid-Holocene anomaly relative to the preindustrial simulation (E , F , T_{ini} and q_{ini}).

3.2. Mechanisms of Enhanced Mid-Holocene Precipitation

Given the profound effect of changing E on the mid-Holocene North African precipitation, we ran a simulation with only one change from REV: increasing E from its default value of 0 to 0.25. Figure 3a shows the percentage difference in the mid-Holocene minus preindustrial (6 kaGS–0 ka) precipitation anomalies for the pair of simulations with $E = 0.25$ compared to the pair with $E = 0$. With $E = 0.25$ the precipitation anomaly is generally larger across North Africa and is nearly twice as large in the North West (Figure 3a). The latitude of the precipitation maximum moves northwards by around 2.5–5° compared to the $E = 0$ simulation (not shown). It produces a more diffuse precipitation band during JJAS which pushes the periphery of the monsoon further into the dry interior.

A key diagnostic of the convection scheme is the updraught mass-flux. The simulated mean convective updraught over North Africa decreases fractionally much more with height than the mean over the wet regions of the tropics as a whole. This is presumably because of dilution by the extremely dry environment in North Africa, which makes it harder for moist convective plumes to persist. In all model versions the

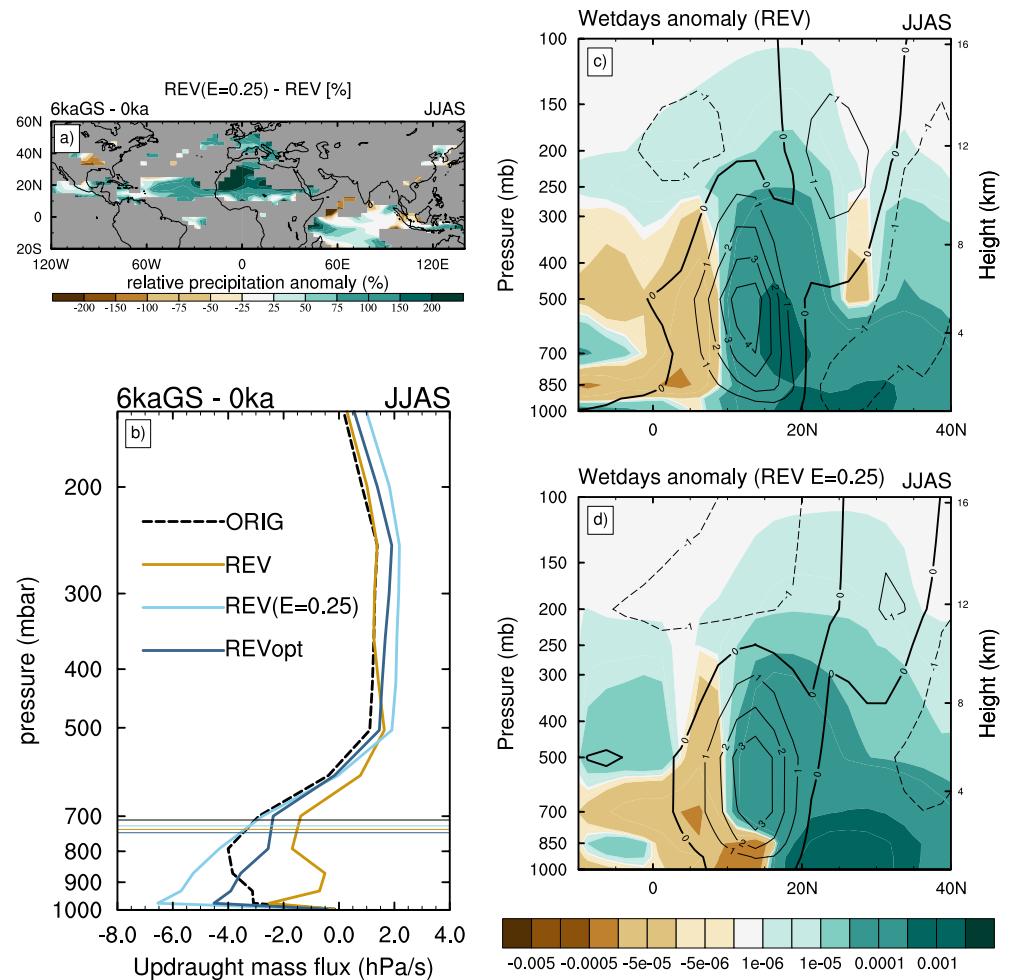


Figure 3. (a) relative difference in the mid-Holocene JJAS precipitation anomaly (6kaGS-0ka) for REV model version $E = 0.25$ minus $E = 0$. (b) Mid-Holocene minus preindustrial (6 kaGS-0 ka) JJAS mean vertical profiles of updraught mass flux (hPa s^{-1}). Horizontal lines show the lifting condensation level for an undilute parcel of surface air for the mid-Holocene averaged over the same domain. (c) and (d) The REV JJAS zonally averaged daily mean anomalies of humidity (shading: kg kg^{-1}) and zonal wind (contour lines: ms^{-1}) for wetdays ($>4.0 \text{ mm day}^{-1}$) for $E = 0$ and $E = 0.25$ respectively.

increase in rainfall over North Africa at 6 ka BP is accompanied by the updraught mass flux weakening lower down and strengthening aloft (Figure 3b), becoming more like tropical moist convection elsewhere in the tropics. The mid-Holocene boundary conditions lead to less dilution of convective plumes low down, so that those that reach their lifting condensation level (LCL: indicated by vertical lines in Figure 3b) are more vigorous and end up penetrating higher overall.

The direct effect of increasing the parameter E , that is, decreasing the entrainment rate near the surface and increasing entrainment rate higher up, is to amplify these mass flux changes for the mid-Holocene relative to the preindustrial (Figure 3b), so that the REV ($E = 0.25$) case has a lower mass-flux near the surface than the REV model version, and a stronger updraught mass flux above the lifting condensation level (LCL: indicated by vertical lines in Figure 3b). Interactions between convection and its environment mean the net effect can be very different in other regions (Figure 3a), but over North Africa these changes reinforce each other to produce larger amplitude mass flux changes, and a stronger rainfall increase at 6 ka BP (Figure 3d).

In tandem with this, the circulation (zonal wind) and humidity anomalies associated with heavier downpours in the Sahara are different when E is given a higher value (Figures 3c and 3d). For $E = 0$, wetter days north of 15°N are associated with a strengthened tropical easterly jet (TEJ) and a slightly weakened Africa

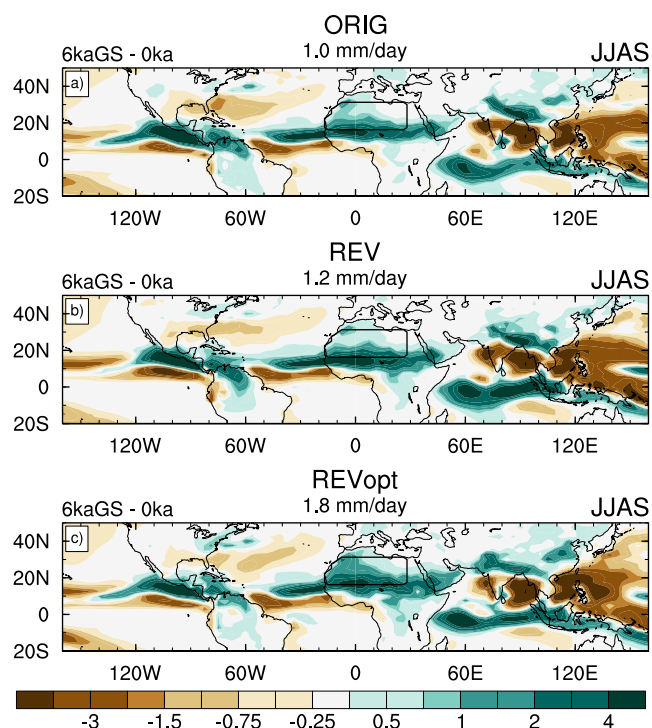


Figure 4. Simulated Northern Hemisphere summer (JJAS) precipitation anomalies (mm day^{-1}): (a) ORIG (Valdes et al., 2017); (b) REV: the modified version used as a starting configuration in this study; and (c) REVopt, the optimized version based on the probabilistic approach. The mean simulated difference in JJAS precipitation (mm day^{-1}) for North Africa in the area of the box is given above each panel.

easterly jet (AEJ), as observed (Nicholson, 2009). African Easterly Waves (AEWs) move along the jet and contribute precipitation to the North (Claussen et al., 2017) and this is well represented in HadAM3 (Taylor et al., 2002). For $E = 0.25$, the same precipitation increase is achieved with a 20% smaller increase in the TEJ. This suggests that convection is more effective in this model configuration and this partly explains the increased precipitation response for $E = 0.25$. Some of these downpours are also associated with tropical plumes (Knippertz, 2003), especially in the months of August–October (Dallmeyer et al., 2020; Skinner & Poulsen, 2016). When E is increased to 0.25, plumes contribute more precipitation in the region from 20–35°N despite relatively similar mean climatologies of large-scale circulation and humidity.

3.3. Learning from the Model-Data Mismatch

The mid-Holocene pollen quantitative precipitation reconstruction over North Africa gives an annual-mean precipitation increase of $1.1 \pm 0.1 \text{ mm day}^{-1}$ (Bartlein et al., 2011) relative to the present day. We use the annual mean reconstruction and model outputs in a probabilistic formulation to optimize the GCM so that it is consistent with the pollen-based precipitation reconstructions and hence the widespread environmental evidence for an invigoration of the hydrological cycle.

The posterior PDFs on the 11 parameters are shown in Figure S6. Two cases are considered where the second only differs with the inclusion of the mid-Holocene precipitation target. For the mid-Holocene the algorithm favors high E because as discussed above, it has an extremely strong impact on the response to the mid-Holocene insolation. The emulator predicted mid-Holocene precipitation increase is very different between the two cases, showing sensitivity of the system to parameter combinations and also that the optimization against present-day observations does not guarantee an improvement for the mid-Holocene.

3.4. New Model Version

One optimized parameter set derived from the PDFs on the model parameters (Figure S6 and Tables S4 and S5) was used in new preindustrial and mid-Holocene GCM simulations and is denoted REVopt. In this we only changed parameters from their original GCM values where there is stronger preference posterior PDF. Whilst the choice of parameters which underline REVopt is based on the posterior PDF sampling, it would be more consistent with the Bayesian paradigm to think in terms of the probability distribution on the parameters, rather than to focus on any single parameter set. However, given computational limitations and to simplify the presentation of the results we mostly focus on the REVopt parameter set.

This simulation is compared with the ORIG and REV models in Figure 4. The difference between the two controls (ORIG and REV) is due to changes to the detrainment parametrization following Derbyshire et al. (2011). Figure 4c shows that in REVopt the precipitation anomaly over North Africa is approaching double that in the ORIG simulations for JJAS, and the annual mean anomaly is also 67% larger. There is a large region of precipitation increase across North Africa and Arabia and Northern India. This shows that the statistically-inferred parameter changes are effective when introduced into the GCM. Crucially, the present-day performance of REVopt is very similar to ORIG and REV for both temperature and precipitation (supporting information Text S4 and Figures S7 and S8). This means that the improvement for the mid-Holocene has not significantly altered the present-day simulation.

4. Discussion

The strong precipitation increase during the early- to mid-Holocene in North Africa presents a unique challenge to climate simulations of tropical precipitation. In this perturbed parameter study we find that parameters controlling the preindustrial climatology of precipitation are different from those that determine the anomaly under a climate change scenario. The Bayesian approach demonstrates that a modified vertical profile of convective entrainment can significantly improve the simulation of the mid-Holocene North Africa despite having little impact on the simulation of the present day.

Like any model, HadCM3 has biases and simplifications. For example, HadCM3 suffers from having too little, too optically bright cloud cover (Massey et al., 2015), a common problem in CMIP5 models (Nam et al., 2012). It also has too much precipitation over Africa and too little over South America, but does not suffer from a double ITCZ bias or weak ENSO variability, which are common problems in many GCMs. Overall its performance compared to observations is typical of GCMs used in recent intercomparisons (Valdes et al., 2017).

Structural limitations mean that many biases could be corrected by varying model parameters, and there are many more than the 11 we varied. Also, the existence of compensating errors means that tuning that improves one bias can actually exacerbate another. Despite this, in the REVOpt case we significantly improved the mid-Holocene precipitation in comparison with reconstructions, without affecting the simulation of the present day state. It is possible that with a more comprehensive list of parameters, for example, of the order of 20–50, some of these other biases may be reduced.

Tropical precipitation in GCMs has recently been improved through the use of adaptive convective entrainment, whereby local entrainment rates reduce following convective activity. On a local scale this could produce a similar effect as in our study, reducing entrainment in the lower troposphere, following precursor convective plumes (Mapes & Neale, 2011; Willett & Whittall, 2017). Future work should consider how such dynamic entrainment parametrizations (e.g., Hohenegger & Bretherton, 2011; Mapes & Neale, 2011) could similarly improve modeling of the mid-Holocene and whether this is consistent with our statistically derived model changes.

Convection-permitting atmospheric model simulations, with high resolution and no convection parametrization, have highlighted further significant improvements when convection parametrizations are deactivated (Berthou et al., 2019; Birch et al., 2014; Finney et al., 2019; Kendon et al., 2019; Marsham et al., 2013; Pante & Knippertz, 2019). This includes a more realistic diurnal cycle of precipitation (Marsham et al., 2013), improved simulation of wet spells (Berthou et al., 2019; Kendon et al., 2019) and of cloud cover and humidity (Pante & Knippertz, 2019). Making this transition is not without drawbacks and substantial model errors can emerge (Pante & Knippertz, 2019) that are difficult to eliminate because of the high computational cost of test simulations. Future work could compare convection-permitting simulations and ensembles of GCM simulations like those studied here for both present day and paleoclimate conditions to identify further ways to improve GCM parametrization schemes.

Some have argued that the Green Sahara modeling problem may be resolved by altering model boundary conditions such as vegetation coverage or dust loading (Chandan & Peltier, 2020; Pausata et al., 2016). Here, we have shown that it is also possible to improve the simulation of precipitation through changes to the model parametrizations, many aspects of which are subject to significant uncertainty. This focus on the model itself would strengthen the rationale for evaluating the relationship between past and future climate change, given that very different boundary conditions characterize the past and future (orbital changes for the mid-Holocene, vs. greenhouse gases and land use for the near future). Some earlier (Claussen & Gayler, 1997) and more recent model studies (Dallmeyer et al., 2020) have successfully simulated the Green Sahara without prescribing large changes to the land-surface. We speculate that this shows that for a limited number of GCMs the convection schemes are compatible with these paleoclimatic states. In most other models including HadCM3 used here, the convection scheme may need to be specifically tuned. It would be informative to test the impacts of similar entrainment changes in other models, in transient Holocene simulations and under future climate scenarios.

5. Conclusions

Most climate models are developed and calibrated against modern climate. We have shown that there are multiple parameter sets which allow for a good simulation of the present day conditions, but that only a subset of these are also able to satisfy past criteria. This example provides a new quantitative demonstration of how a paleoclimate state may provide information of relevance to uncertainty in simulating future precipitation change. Paleoclimate may therefore be a significantly undervalued source of additional information for informing the parameter values and parametrization choices in GCMs as it has rarely been used in this way, see examples by Hopcroft and Valdes (2015) and DiNezio et al. (2016). Well documented climate states in the past thus may have the potential to be used in model development and this approach can include other important paleoclimate changes.

Data Availability Statement

The Met Office released the HadCM3 source code via the Ported Unified Model release (<https://www.metoffice.gov.uk/research/approach/collaboration/unified-model/partnership>, and um_collaboration@metoffice.gov.uk). Code modifications required to produce the ORIG version of HadAM3/HadCM3 are available from <https://doi.org/10.5194/gmd-10-3715-2017>. The HadAM3/HadCM3 code changes for the REV and REVOpt model versions and the parameter namelist files required to configure these simulations are available from figshare: <https://doi.org/10.6084/m9.figshare.12311360>. The ensemble simulation output analyzed in the study are available from www.paleo.bristol.ac.uk/ummodel/scripts/papers/. The netcdf climatologies of the preindustrial and mid-Holocene ORIG, REV and REVOpt simulations are available from figshare <https://doi.org/10.6084/m9.figshare.12505259>. The statistical emulator is available in the R package DiceKriging. The Bartlein et al. (2011) mid-Holocene pollen-based climate reconstruction is available from pmip3.lsce.ipsl.fr. The Tierney et al. (2017) precipitation reconstruction is available from <http://www.ncdc.noaa.gov/paleo/study/21091>. CRU precipitation is available from <https://crudata.uea.ac.uk/cru/data/hrg/>. CERES land surface albedo is available from <https://ceres.larc.nasa.gov/data/>. GPCP precipitation is available from dx.doi.org/10.7289/V56971M6.

Acknowledgments

P. O. Hopcroft was funded by the EPSRC-funded Past Earth Network Feasibility Study (Grant number EP/M008363/1) and by a University of Birmingham Fellowship. W. Ingram was supported by the Met Office Hadley Center Climate Program funded by BEIS and Defra. This work was carried out using the computational facilities of the Birmingham Environment for Academic Research, <http://www.bear.bham.ac.uk> and the Advanced Computing Research Center, University of Bristol, <http://www.bris.ac.uk/acrc>. The authors thank Gethin Williams for installing the climate model code on BEAR.

References

- Albani, S., & Mahowald, N. (2019). Paleodust insights into dust impacts on climate. *Journal of Climate*, 32, 7897–7913. <https://doi.org/10.1175/JCLI-D-18-0742.1>
- Allen, M., & Ingram, W. (2002). Constraints on future changes in climate and the hydrologic cycle. *Nature*, 419, 224–232.
- Bartlein, P. J., Harrison, S., Brewer, S., Connor, S., Davis, B., Gajewski, K., et al. (2011). Pollen-based continental climate reconstructions at 6 and 21 ka: a global synthesis. *Climate Dynamics*, 37(3–4), 775–802. <https://doi.org/10.1007/s00382-010-0904-1>
- Berger, A., & Loutre, M. (1991). Insolation values for the climate of the last 10 million years. *Quaternary Science Reviews*, 10, 297–317.
- Berthou, S., Rowell, D., Kendon, E., Roberts, M., Stratton, R., et al. (2019). Improved climatological precipitation characteristics over West Africa at convection-permitting scales. *Climate Dynamics*, 53, 1991–2011. <https://doi.org/10.1007/s00382-019-04759-4>
- Biasutti, M., Voigt, A., Boos, W., Braconnot, P., Hargreaves, J. C., Harrison, S. P., et al. (2018). Global energetics and local physics as drivers of past, present and future monsoons. *Nature Geoscience*, 11, 392–400. <https://doi.org/10.1038/s41561-018-0137-1>
- Birch, C., Parker, D., Marsham, J. H., Copsey, D., Garcia-Carreras, L. (2014). A seamless assessment of the role of convection in the water cycle of the West African Monsoon. *Journal of Geophysical Research: Atmospheres*, 119, 2890–2912. <https://doi.org/10.1002/2013JD020887>
- Boos, W., & Storelvmo, T. (2016). Near-linear response of mean monsoon strength to a broad range of radiative forcings. *Proceedings of the National Academy of Sciences*, 113, 1510–1515. <https://doi.org/10.1073/pnas.1517143113>
- Braconnot, P., Harrison, S., Kageyama, M., Bartlein, P., Masson-Delmotte, V., Abe-Ouchi, A., et al. (2012). Evaluation of climate models using palaeoclimatic data. *Nature Climate Change*, 2, 417–424. <https://doi.org/10.1038/nclimate1456>
- Braconnot, P., Otto-Bliesner, B., Harrison, S., Joussaume, S., Peterchmitt, J.-Y., Abe-Ouchi, A., et al. (2007). Results of PMIP2 coupled simulations of the Mid-Holocene and Last Glacial Maximum Part 1: Experiments and large-scale features. *Climate of the Past*, 3, 261–277. <https://doi.org/10.5194/cp-3-261-2007>
- Brierley, C., Zhao, A., Harrison, S., Braconnot, P., Williams, C. J. R., Thornalley, D. J. R., et al. (2020). Large-scale features and evaluation of the PMIP4-CMIP6 midHolocene simulations. *Climate of the Past*, 16, 1847–1872. <https://doi.org/10.5194/cp-16-1847-2020>
- Chadwick, R., Good, P., Martin, G., & Rowell, D. (2016). Large rainfall changes consistently projected over substantial areas of tropical land. *Nature Climate Change*, 6, 177–182. <https://doi.org/10.1038/NCLIMATE2805>
- Chandan, D., & Peltier, W. (2020). African humid period precipitation sustained by robust 2 vegetation, soil and lake feedbacks. *Geophysical Research Letters*, 47, e2020GL088728. <https://doi.org/10.1029/2020GL088728>
- Charney, J. (1975). Dynamics of deserts and drought in the Sahel. *Quarterly Journal of the Royal Meteorological Society*, 101, 193–202. <https://doi.org/10.1002/qj.49710142802>
- Chen, W., Ciais, P., Zhu, D., Ducharme, A., Viovy, N., Qiu, C., Huang, C., et al. (2020). Feedbacks of soil properties on vegetation during the Green Sahara period. *Quaternary Science Reviews*, 240, 106389. <https://doi.org/10.1016/j.quascirev.2020.106389>
- Claussen, M., Dallmeyer, A., & Bader, J. (2017). *Theory and Modeling of the African Humid Period and the Green Sahara* (pp. 1–38). Oxford Research Encyclopedia of Climate Science. <https://doi.org/10.1093/acrefore/9780190228620.013.532>

- Claussen, M., & Gayler, V. (1997). The greening of the Sahara during the Mid-Holocene: Results of an interactive atmosphere- biome model. *Global Ecology and Biogeography Letters*, 6, 369–377.
- Dallmeyer, A., Claussen, M., Lorenz, S., & Shanahan, T. (2020). The end of the African humid period as seen by a transient comprehensive Earth system model simulation of the last 8000 years. *Climate of the Past*, 16, 117–140. <https://doi.org/10.5194/cp-16-117-2020>
- de Menocal, P., Ortiz, J., Guilderson, T., Adkins, J., Sarnthein, M., Baker, L., & Yarusinsky, M. (2000). Abrupt onset and termination of the African Humid Period: rapid climate responses to gradual insolation forcing. *Quaternary Science Reviews*, 19, 347–361.
- Derbyshire, S., Maidens, A., Milton, S., Stratton, R., & Willett, M. (2011). Adaptive detrainment in a convective parametrization. *Quarterly Journal of the Royal Meteorological Society*, 137, 1856–1871. <https://doi.org/10.1002/qj.875>
- DiNezio, P., Timmermann, A., Tierney, J., Jin, F.-F., Otto-Bliesner, B., Rosenbloom, N., et al. (2016). The climate response of the Indo-Pacific warm pool to glacial sea level. *Paleoceanography*, 31, 866–894. <https://doi.org/10.1002/2015PA002890>
- Edwards, T., Brandon, M., Durand, G., Edwards, N. R., Golledge, N. R., Holden, P. B., et al. (2019). Revisiting Antarctic ice loss due to marine ice-cliff instability. *Nature*, 566, 58–64. <https://doi.org/10.1038/s41586-019-0901-4>
- Essery, R., Best, M., Betts, R., Cox, P., & Taylor, C. (2003). Explicit representation of subgrid heterogeneity in a GCM land-surface scheme. *Journal of Hydrometeorology*, 4(3), 530–543. [https://doi.org/10.1175/1525-7541\(2003\)004<0530:EROSHI>2.0.CO;2](https://doi.org/10.1175/1525-7541(2003)004<0530:EROSHI>2.0.CO;2)
- Finney, D., Marsham, J., Jackson, L., Kendon, E. J., Rowell, D. P., Boorman, P. M., et al. (2019). Implications of improved representation of convection for the East Africa water budget using a convection-permitting model. *Journal of Climate*, 32, 2109–2129. <https://doi.org/10.1175/JCLI-D-18-0387.1>
- Gilks, W., Richardson, S., & Spiegelhalter, D. (1995). Introducing Markov chain monte carlo methods. In W. R. Gilks, S. Richardson, & D. J. Spiegelhalter, Eds., *Markov chain Monte Carlo in practice* (p. 512). Chapman and Hall.
- Gordon, C., Cooper, C., Senior, C. A., Banks, H., Gregory, J. M., Johns, T. C., & Wood, R. A. (2000). The simulation of sst, sea ice extents and ocean heat transports in a version of the Hadley Center coupled model without flux adjustments. *Climate Dynamics*, 16, 147–168.
- Gregory, D., & Rowntree, P. (1990). A mass-flux convection scheme with representation of cloud ensemble characteristics and stability dependent closure. *Monthly Weather Review*, 118, 1483–1506.
- Harris, I., Jones, P., Osborn, T., & Lister, D. (2014). Updated high-resolution grids of monthly climatic observations: The CRU TS3.10 Dataset. *International Journal of Climatology*, 34, 623–642. <https://doi.org/10.1002/joc.3711>
- Harrison, S., Bartlein, P., Izumi, K., Li, G., Annan, J., Hargreaves, J., & Kageyama, M. (2015). Evaluation of CMIP5 palaeo-simulations to improve climate projections. *Nature Climate Change*, 5, 735–743. <https://doi.org/10.1038/nclimate2649>
- Hély, C., Lezine, A.-M., & contributors, A. P. D. (2014). Holocene changes in African vegetation: tradeoff between climate and water availability. *Climate of the Past*, 10, 681–686. <https://doi.org/10.5194/cp-10-681-2014>
- Hoegh-Guldberg, O., Jacob, D., Taylor, M., Bindi, M., Brown, S., Camilloni, I., et al. (2018). Impacts of 1.5°C global warming on natural and human systems. In V. Masson-Delmotte, P. Zhai, H.-O. Portner, D. Roberts, et al. (Eds.), *Global Warming of 1.5°C. An IPCC Special Report on the impacts of global warming of 1.5°C above pre-industrial levels and related global greenhouse gas emission pathways, in the context of strengthening the global response to the threat of climate change, sustainable development, and efforts to eradicate poverty* (pp. 1–616). IPCC. <https://www.ipcc.ch/sr15>
- Hoelzmann, P., Jolly, D., Harrison, S. P., Laarif, F., Bonnefille, R., Pachur, H.-J. (1998). Mid-Holocene land-surface conditions in northern Africa and the Arabian Peninsula: A data set for the analysis of biogeophysical feedbacks in the climate system. *Global Biogeochemical Cycles*, 12, 35–51.
- Hohenegger, C., & Bretherton, C. (2011). Simulating deep convection with a shallow convection scheme. *Atmospheric Chemistry and Physics*, 11, 10389–10406. <https://doi.org/10.5194/acp-11-10389-2011>
- Hopcroft, P., & Valdes, P. (2015). Last Glacial Maximum constraints on the Earth System model HadGEM2-ES. *Climate Dynamics*, 45, 1657–1672. <https://doi.org/10.1007/s00382-014-2421-0>
- Hopcroft, P., & Valdes, P. (2019). On the role of dust-climate feedbacks during the mid-Holocene. *Geophysical Research Letters*, 46, 1612–1621. <https://doi.org/10.1029/2018GL080483>
- Hopcroft, P., Valdes, P., Harper, A., & Beerling, D. (2017). Multi vegetation model evaluation of the Green Sahara climate regime. *Geophysical Research Letters*, 44, 6804–6813. <https://doi.org/10.1002/2017GL073740>
- Jolly, D., Prentice, I., Bonnefille, R., Aziz Ballouche, A., Buchet, G., Bengo, M. D., et al. (1998). Biome reconstruction from pollen and plant macrofossil data for Africa and the Arabian peninsula at 0 and 6000 years. *Journal of Biogeography*, 25, 1007–1027.
- Joussaume, S., Taylor, K. E., Braconnot, P., Mitchell, J. F. B., Kutzbach, J. E., Harrison, S. P., et al. (1999). Monsoon changes for 6000 years ago: Results of 18 simulations from the Paleoclimate modeling intercomparison project (PMIP). *Geophysical Research Letters*, 26, 859–862.
- Kendon, E., Stratton, R., Tucker, S., Marsham, J. H., Berthou, S., Rowell, D. P., & Senior, C. A. (2019). Enhanced future changes in wet and dry extremes over Africa at convection-permitting scale. *Nature Communications*, 10, 1794. <https://doi.org/10.1038/s41467-019-09776-9>
- Kennedy, M., & O'Hagan, A. (2001). Bayesian calibration of computer models. *Journal of the Royal Statistical Society B*, 63, 425–464.
- Kent, C., Chadwick, R., & Rowell, D. (2015). Understanding uncertainties in future projections of seasonal tropical precipitation. *Journal of Climate*, 28, 4390–4413. <https://doi.org/10.1175/JCLI-D-14-00613.1>
- Knippertz, P. (2003). Tropical-extratropical interactions causing precipitation in northwest Africa: Statistical analysis and seasonal variations. *Monthly Weather Review*, 131, 3069–3076. [https://doi.org/10.1175/1520-0493\(2003\)131<3069:TICPIN>2.0.CO;2](https://doi.org/10.1175/1520-0493(2003)131<3069:TICPIN>2.0.CO;2)
- Kohfeld, K., & Harrison, S. (2000). How well can we simulate past climates? Evaluating the models using palaeoenvironmental datasets. *Quaternary Science Reviews*, 19, 321–346.
- Kutzbach, J., & Street-Perrott, F. (1985). Milankovitch forcing of fluctuations in the level of tropical lakes from 18 to 0 kyr BP. *Nature*, 317, 130–134.
- Levis, S., Bonan, G., & Bonfils, C. (2004). Soil feedback drives the mid-Holocene North African monsoon northward in fully coupled CCSM2 simulations with a dynamic vegetation model. *Climate Dynamics*, 23, 791–802. <https://doi.org/10.1007/s00382-004-0477-y>
- Loeb, N., Lyman, J., Johnson, G., Allan, R., Doeling, D., Wong, T., & Stephenes, G. (2012). Observed changes in top-of-the-atmosphere radiation and upper-ocean heating consistent within uncertainty. *Nature Geoscience*, 5, 110–113. <https://doi.org/10.1038/ngeo1375>
- Loveland, T., Reed, B., Brown, J., Ohlen, D., Zhu, Z., Yang, L., & Merchant, J. (2000). Development of a global land cover characteristics database and IGBP DISCover from 1 km AVHRR data. *International Journal of Remote Sensing*, 21(6–7), 1303–1330
- Lu, Z., Miller, P., Zhang, Q., Wärlind, D., Nieradzki, L., Sjolte, J., et al. (2018). Dynamic vegetation simulations of the mid-Holocene Green Sahara. *Geophysical Research Letters*, 45, 1–10. <https://doi.org/10.1029/2018GL079195>
- Manning, K., & Timpson, A. (2014). The demographic response to Holocene climate change in the Sahara. *Quaternary Science Reviews*, 101, 28–35. <https://doi.org/10.1016/j.quascirev.2014.07.003>

- Mapes, B., & Neale, R. (2011). Parameterizing convective organization to escape the entrainment dilemma. *Journal of Advances in Modeling Earth Systems*, 3, M06004. [10.1029/2011MS000042](https://doi.org/10.1029/2011MS000042)
- Maraun, D., & Widmann, M. (2018). *Statistical downscaling and bias correction for climate research* (1st ed., p. 347). Cambridge University Press. <https://doi.org/10.1017/9781107588783>
- Marsham, J., Dixon, N., Garcia-Carreras, L., Lister, G. M. S., Parker, D. J., Knippertz, P., Birch, C. E. (2013). The role of moist convection in the West African monsoon system: Insights from continental-scale convection-permitting simulations. *Geophysical Research Letters*, 40, 1843–1849. <https://doi.org/10.1002/grl.50347>
- Massey, N., Jones, R., Otto, F., Aina, T., Wilson, S., Murphy, J. M., et al. (2015). weather@home development and validation of a very large ensemble modeling system for probabilistic event attribution. *Quarterly Journal of the Royal Meteorological Society*, 14, 1528–1545. <https://doi.org/10.1002/qj.2455>
- McKay, M., Beckman, R., & Conover, W. (1979). A comparison of three methods for selecting values of input variables in the analysis of output from a computer code. *Technometrics*, 32, 239–245.
- McNeill, D., Williams, J., Booth, B., Betts, R., Challenor, P., Wiltshire, A., & Sexton, D. (2016). The impact of structural error on parameter constraint in a climate model. *Earth System Dynamics Discussions*, 7, 917–935. [10.5194/esd-2016-17](https://doi.org/10.5194/esd-2016-17)
- Nam, C., Bony, S., Dufresne, J.-L., & Chepfer, H. (2012). The 'too few, too bright' tropical low-cloud problem in cmip5 models. *Geophysical Research Letters*, 39, L21801. <https://doi.org/10.1029/2012GL053421>
- Nicholson, S. (2009). A revised picture of the structure of the monsoon and land ITCZ over West Africa. *Climate Dynamics*, 32, 1155–1171. <https://doi.org/10.1007/s00382-008-0514-3>
- Pachur, H.-J., & Holzmann, P. (1991). Paleoclimatic implications of late quaternary lacustrine sediments in Western Nubia, Sudan. *Quaternary Research*, 36, 257–276.
- Pante, G., & Knippertz, P. (2019). Resolving Sahelian thunderstorms improves mid-latitude weather forecasts. *Nature Communications*, 10, 3487. <https://doi.org/10.1038/s41467-019-11081-4>
- Pausata, F., Messori, G., & Zhang, Q. (2016). Impacts of dust reduction on the northward expansion of the African monsoon during the Green Sahara period. *Earth and Planetary Science Letters*, 434, 298–307. <https://doi.org/10.1016/j.epsl.2015.11.049>
- Perez-Sanz, A., Li, G., Gonzalez-Samperiz, P., & Harrison, S. (2014). Evaluation of modern and mid-Holocene seasonal precipitation of the Mediterranean and northern Africa in the CMIP5 simulations. *Climate of the Past*, 10, 551–568. [10.5194/cp-10-551-2014](https://doi.org/10.5194/cp-10-551-2014)
- Peyron, O., Jolly, P., Braconnot, P., Bonnefille, R., Guiot, J., Wirmann, D., & Chalé, F. (2006). Quantitative reconstructions of annual rainfall in Africa 6000 years ago: Model-data comparison. *Journal of Geophysical Research*, 111, D24110. <https://doi.org/10.1029/2006JD007396>
- Pope, V. D., Gallani, M. L., Rowntree, P. R., & Stratton, R. A. (2000). The impact of new physical parametrizations in the Hadley Center climate model: HadAM3. *Climate Dynamics*, 16, 123–146.
- Rayner, N., Parker, D., Horton, E., Folland, C., Alexander, L., Rowell, D., & Kaplan, A. (2003). Global analyses of sea surface temperature, sea ice, and night marine air temperature since the late nineteenth century. *Journal of Geophysical Research*, 108(D14), 4407. <https://doi.org/10.1029/2002JD002670>
- Ritchie, J., & Haynes, C. (1987). Holocene vegetation zonation in the eastern Sahara. *Nature*, 330, 645–647.
- Rougier, J. (2007). Probabilistic inference for future climate using an ensemble of climate model evaluations. *Climatic Change*, 81, 247–264. <https://doi.org/10.1007/s10584-006-9156-9>
- Rougier, J., Sexton, D., Murphy, J., & Stainforth, D. (2009). Analyzing the climate sensitivity of the hadsm3 climate model using ensembles from different but related experiments. *Journal of Climate*, 22, 1327–1353. <https://doi.org/10.1175/2008JCLI2533.1>
- Roustant, O., Ginsbourger, D., & Deville, Y. (2012). DiceKriging, DiceOptim: Two R packages for the analysis of computer experiments by Kriging-based metamodeling and optimization. *Journal of Statistical Software*, 51, 1–55. [10.18637/jss.v051.i01](https://doi.org/10.18637/jss.v051.i01)
- Rowell, D., Senior, C., Vellinga, M., & Graham, R. (2016). Can climate projection uncertainty be constrained over Africa using metrics of contemporary performance? *Climatic Change*, 134, 621–633. <https://doi.org/10.1007/s10584-015-1554-4>
- Schmidt, G., Annan, J., Bartlein, P., Cook, B., Guilyardi, E., Hargreaves, J., & Yiou, P. (2014). Using palaeo-climate comparisons to constrain future projections in CMIP5. *Climate of the Past*, 10, 221–250. <https://doi.org/10.5194/cp-10-221-2014>
- Sexton, D., Murphy, J., Collins, M., & Webb, M. (2012). Multivariate probabilistic projections using imperfect climate models part I: Outline of methodology. *Climate Dynamics*, 38, 2513–2542. [10.1007/s00382-011-1208-9](https://doi.org/10.1007/s00382-011-1208-9)
- Skinner, C., & Poulsen, C. (2016). The role of fall season tropical plumes in enhancing Saharan rainfall during the African Humid Period. *Geophysical Research Letters*, 43, 349–358. <https://doi.org/10.1002/2015GL066318>
- Skonieczny, C., Paillou, A., Bory, P., Bayon, G., Biscara, L., Crosta, X., et al. (2015). African humid periods triggered the reactivation of a large river system in Western Sahara. *Nature Communications*, 6, 8751–8756. [10.1038/ncomms9751](https://doi.org/10.1038/ncomms9751)
- Stensrud, D. (2007). *Parameterization schemes: Keys to understanding numerical weather prediction models* (1st ed., p. 459). Cambridge, UK: Cambridge University Press.
- Street-Perrott, F., Mitchell, J., Marchand, D., & Brunner, J. (1990). Milankovitch and albedo forcing of the tropical monsoons: A comparison of geological evidence and numerical simulations for 9000 yBP. *Earth and Environmental Science Transactions of the Royal Society of Edinburgh*, 81, 407–427.
- Su, H., & Neelin, J. (2005). Dynamical mechanisms for African monsoon changes during the mid-Holocene. *Journal of Geophysical Research*, 110, D19105. <https://doi.org/10.1029/2005JD005806>
- Taylor, C., Lambin, E., Stephenne, N., Harding, R. J., & Essery, R. L. H. (2002). The influence of land use change on climate in the Sahel. *Journal of Climate*, 15(24), 3615–3629. [10.1175/1520-0442\(2002\)015<3615:TIOLOC>2.0.CO;2](https://doi.org/10.1175/1520-0442(2002)015<3615:TIOLOC>2.0.CO;2)
- Texier, D., De Noblet, N., & Braconnot, P. (2000). Sensitivity of the African and Asian Monsoons to Mid-Holocene Insolation and Data-Inferred Surface Changes. *Journal of Climate*, 13, 164–181.
- Thompson, A., Skinner, C., Poulsen, C., & Zhu, J. (2019). Modulation of mid-holocene african rainfall by dust-aerosol direct and indirect effects. *Geophysical Research Letters*, 46, 3917–3926. <https://doi.org/10.1029/2018GL081225>
- Thompson, A., Tabor, C., Poulsen, C., & Skinner, C. (2021). Water isotopic constraints on the enhancement of the mid-Holocene West African monsoon. *Earth and Planetary Science Letters*, 554, 116677. <https://doi.org/10.1016/j.epsl.2020.116677>
- Tierney, J., Pausata, F., & deMenocal, P. (2017). Rainfall regimes of the Green Sahara. *Science Advances*, 3, e1601503. [10.1126/sciadv.1601503](https://doi.org/10.1126/sciadv.1601503)
- Tierney, J., Poulsen, C., Montanez, I., Bhattacharya, T., Ford, H. L., Feng, R., et al. (2020). Past climates inform our future. *Science*, 370, eaay3701. <https://doi.org/10.1126/science.aay3701>
- Valdes, P. (2011). Built for stability. *Nature Geoscience*, 4, 414–416. <https://doi.org/10.1038/ngeo1200>
- Valdes, P., Armstrong, E., Badger, M., Bradshaw, C., Bragg, F., Crucifix, M., & Williams, J. (2017). The BRIDGE HadCM3 family of climate models: HadCM3@Bristol v1.0. *Geoscientific Model Development*, 10, 3715–3743. <https://doi.org/10.5194/gmd-10-3715-2017>

- Vamborg, F., Brovkin, V., & Claussen, M. (2011). The effect of a dynamic background albedo scheme on Sahel/Sahara precipitation during the mid-Holocene. *Climate of the Past*, 7, 117–131. <https://doi.org/10.5194/cp-7-117-2011>
- Willett, M., & Whittall, M. (2017). A simple prognostic based convective entrainment rate for the Unified Model: Description and tests. Forecasting Research Technical Report (Vol. 617, pp. 1–54). Met Office.
- Williams, R., McGee, D., Kinsley, C., Ridley, D., Hu, S., Fedorov, A., et al. (2016). Glacial to holocene changes in trans-Atlantic Saharan dust transport and dust-climate feedbacks. *Science Advances*, 2, e1600445. <https://doi.org/10.1126/sciadv.1600445>
- Wu, H., Guiot, J., Brewer, S., & Guo, Z. (2007). Climatic changes in Eurasia and Africa at the last glacial maximum and mid-Holocene: Reconstruction from pollen data using inverse vegetation modeling. *Climate Dynamics*, 29, 211–229. <https://doi.org/10.1007/s00382-007-0231-3>
- Zhu, J., CJ, P., & Otto-Bliesner, B. (2020). High climate sensitivity in CMIP6 model not supported by paleoclimate. *Nature Climate Change*, 10, 378–379. <https://doi.org/10.1038/s41558-020-0764-6>

References From the Supporting Information

- Adler, R., Sapiiano, M., Huffman, G. J., Wang, J., Gu, G., Bolvin, D., et al. (2003). The Version-2 Global Precipitation Climatology Project (GPCP) monthly precipitation analysis (1979present). *Journal of Hydrometeorology*, 4(6), 1147–1167. [https://doi.org/10.1175/1525-7541\(2003\)004<1147:TVGPCP>2.0.CO;2](https://doi.org/10.1175/1525-7541(2003)004<1147:TVGPCP>2.0.CO;2)
- Bonan, G. (2015). *Ecological climatology* (p. 678, 3rd ed.). Cambridge University Press.
- Fritsch, J., & Chappell, C. (1980). Numerical prediction of convectively driven mesoscale pressure systems. Part I: convective parameterization. *Journal of the Atmospheric Sciences*, 37, 1722–1733.
- Harris, I., Jones, P., Osborn, T., & Lister, D. (2014). Updated high-resolution grids of monthly climatic observations: The CRU TS3.10 Dataset. *International Journal of Climatology*, 34, 623–642. <https://doi.org/10.1002/joc.3711>
- Harrison, S., Bartlein, P., Brewer, S., Prentice, I., Boyd, M., Hessler, I., et al. (2014). Climate model benchmarking with glacial and mid-Holocene climates. *Climate Dynamics*, 43, 671–688. <https://doi.org/10.1007/s00382-013-1922-6>
- Hegglin, M., Plummer, D., Shepherd, T., Scinocc, J., Anderson, J., Froidevaux, L., et al. (2014). Vertical structure of stratospheric water vapor trends derived from merged satellite data. *Nature Geoscience*, 7, 768–766. <https://doi.org/10.1038/ngeo2236>
- Jones, P., & Harpham, C. (2013). Estimation of the absolute surface air temperature of the Earth. *Journal of Geophysical Research*, 118, 3213–3217. <https://doi.org/10.1002/jgrd.50359>
- Joshi, M., Webb, M., Maycock, A., & Collins, M. (2010). Stratospheric water vapor and high climate sensitivity in a version of the HadSM3 climate model. *Atmospheric Chemistry and Physics*, 10, 7161–7167. <https://doi.org/10.5194/acpd-10-6241-2010>
- Lowe, J., Bernie, D., Bett, P., Brichenol, L., Brown, S., Calvert, D., et al. (2018). *UK Climate Projections UKCP18 Science Overview Report*, v2 (pp. 1–73). Met Office Hadley Centre.
- Murphy, J. M., Sexton, D. M. H., Barnett, D. N., Jones, G. S., Webb, M. J., & Collins, M. (2004). Quantification of modeling uncertainties in a large ensemble of climate change simulations. *Nature*, 430, 768–772. <https://doi.org/10.1038/nature02771>
- New, M., Lister, D., Hulme, M., & Makin, I. (2002). A high-resolution data set of surface climate over global land areas. *Climate Research*, 21(1), 1–25. <https://doi.org/10.3354/cr021001>
- Reichler, T., & Kim, J. (2008). How well do coupled models simulated today's climate? *Bulletin of the American Meteorological Society*, 89, 303–311. <https://doi.org/10.1175/BAMS-89-3-303>
- Sanderson, B., Shell, K., & Ingram, W. (2010). Climate feedbacks determined using radiative kernels in a multi-thousand member ensemble of AOGCMs. *Climate Dynamics*, 35, 1219–1236. <https://doi.org/10.1007/s00382-009-0661-1>
- Schaller, N., Alison, K., Lamb, R., Vautard, R., Yiou, P., Ashpole, I., et al. (2016). Human influence on climate in the 2014 southern England winter floods and their impacts. *Nature Climate Change*, 6, 627–634. <https://doi.org/10.1038/nclimate2927>
- Sime, L., Hopcroft, P., & Rhodes, R. (2019). Impact of abrupt sea ice loss on Greenland water isotopes during the last glacial period. *Proceedings of the National Academy of Sciences*, 116, 4099–4104. <https://doi.org/10.1073/pnas.1807261116>
- Sun, Q., Miao, C., Duan, Q., Ashouri, H., Sorooshian, S., & Hsu, K.-L. (2018). A review of global precipitation data sets: Data sources, estimation, and intercomparisons. *Reviews of Geophysics*, 56, 79–107. <https://doi.org/10.1002/2017RG000574>
- Taylor, K. (2001). Summarizing multiple aspects of model performance in a single diagram. *Journal of Geophysical Research*, 106, 7183–7192.